2024SPSBIC0061

Application of Diffusion Magnetic Resonance Equation in the Detection of Tracheomalacia

***Ibrahim J. A.** [1], **Yusuf S. I.** [2], **Jimoh O. R.** [3] **and M. T. Momoh**[4]
[1-3]Department of Mathematics, Federal University of Technology, Minna, Nigeria.
Department of Health and Allied Sciences Cosmopolitan University, FCT, Abuja, Nigeria.
***Contact e-mail.:** ibrahimjeremiaha@gmail.com
Phone number: 08062164603

Abstract
This research examines the application of Magnetic Resonance Equation in the detection of a disease called Tracheomalacia. The mathematical model applied evolved from the fundamental Bloch equations and was transformed into general flow equations. With appropriate boundary conditions, the method of separation of variables was used to obtain the solutions in two cases: Case 1 – free flow situation and Case 2 – diseased situation. The solution obtained was graphically plotted. From the graphs, the values of magnetization exhibited by the free flow demonstrated free induction decay (FID) with a range of value of 1.26026E-05 to 0.18 while those exhibited by the diseased situation manifest a deformity with a range of value of 1.26026E-05 to 1.5. As shown mathematically from the work, MRI has become an important tool in non-invasive methods of diagnosis and treatment in humans.

Keywords: Bronchoscopy, Magnetization, Relaxation Time, Spine, Tracheomalacia.

1.0 Introduction

Tracheomalacia is a disorder which occurs when the cartilage that maintains the airway (trachea) opens and becomes brittle, causing the trachea to partially collapse, especially during periods of excessive airflow. The most common age groups for this illness are newborns and young children. The typical symptom is stridor upon exhaling. Typically, this is referred to as a collapsed windpipe. Normally, the trachea slightly widens during inhalation and somewhat closes during exhalation. Tracheobronchomalacia is the term used when the disorder affects the big airways (bronchi). Laryngomalacia, a related disorder, can also affect the larynx.

Tracheomalacia may be congenital or acquired later which is known as secondary tracheomalacia. When the trachea's walls give way, it is called tracheomalacia. This may occur as a result of something pressing against the windpipe or weak windpipe walls. The trachealis muscle may be hypotonic in this case (Wert *et al*., 2017). It can affect the entire windpipe or only a small portion of it. Bronchomalacia is the medical term for a deflated portion of the windpipe that extends past the point at which it divides into the two lungs. Noisy breathing is one of the symptoms inside the lung.

Bronchography offers a dynamic and morphological assessment of the tracheobronchial tree along with an accurate measurement of the airway lumen. However, to do this, contrast material must be injected into the constricted airway. Risks can include an allergic response, blockage of the airway, or total obstruction (Fraga *et al*., 2016).

Over the years, Magnetic Resonance Imaging (MRI) is being used to detect partial and total blockage of oxygen flow in the human trachea (which is approximately cylindrical in shape). In recent time, MRI has emerged as an important instrument for functional ventilation imaging, Kauczor *et al*. (2001). After the advent of MRI, deaths from partial or total blockage of the trachea have decreased due to early detection by the use of MRI machines.

Diffusion Magnetic Resonance Imaging (DMRI) is one of the MRI methods that is evolving rapidly. This method offers an accurate assessment of the individual component or multi-component systems in a matter of minutes, as opposed to conventional radioactive tracer methods, which might take weeks for each component (Awojoyogbe *et al*., 2011). The Bloch MRI flow equations and solution can be used to calculate the coefficient of diffusion in terms of the flow parameters. These factors play a crucial role in the study of flow in restricted geometries. This has been used in biological flow, catalysis, the

movement of different materials, the movement of fluids in hydrocarbon reservoirs, the movement of ground water, and the movement of pollutants (Awojoyogbe, 2009).

The amount of material that diffuses in a specific amount of time, or a substance's coefficient of diffusion, is crucial for MRI pipe obstruction detection. The fascinating characteristics of water molecules' random diffusion motion are influenced by the physiological and anatomical surroundings of the animals under study. This idea serves as the foundation for the DMRI method. Due to distinctive relaxation rates, nuclear magnetic resonance may assess the diffusion movement of molecules (Yusuf *et al*., 2010).

Each molecule of water, which has the chemical formula H_2O, includes two hydrogen atoms. Humans are fortunate to have a large number of hydrogen atoms in our bodies for imaging reasons. 60% of an adult's body is made up of water on average. Hydrogen atoms are widely distributed in the energy-storing compounds found in fat and carbohydrate molecules. As a result, Magnetic Resonance Imaging is a useful imaging technique for studying the internal organization of the body (Klioze, 2013).

MRI scanners are particularly well suited to image the non-bony parts or soft tissues of the body. They differ from computed tomography (CT), because they do not use the damaging ionizing radiation of x-rays. Klioze (2013) commented that the brain, spinal cord and nerves, as well as muscles, ligaments and tendons are seen much more clearly with MRI than with regular x-rays and CT; for this reason, MRI is often used to image knee and shoulder injuries.

Nearly every part of the body may be studied with MRI. It gives very detailed pictures of soft tissues like the brain. Magnetic resonance imaging is routinely used in clinical practice to detect and monitor inflammatory lesions in patients with multiple sclerosis (MS) - Tomassini *et al.* (2009). Air and hard bone do not give an MRI signal, so, these areas appear black. Bone marrow, spinal fluid, blood and soft tissues vary in intensity from black to white, depending on the amount of fat and water present in each tissue and the machine settings used for the scan. The radiologist compares the size and distributions of these bright and dark areas to determine whether a tissue is healthy.

Computed tomography originally perceived as standard for assessment of lung morphology and the most reliable imaging modality for monitoring cystic fibrosis (CF) lung disease, (Davis *et al*., 2007) have been implicated with numerous risk factors. CT has a much higher radiation exposure than chest x-ray. The cumulative radiation dose for life-long repeated CT scans has limited its use for CF patients as their life expectancy increases. Clearly, no dose would be preferable over low dose when the same or more relevant information can be obtained.

Until the mid-1990s, chest x-ray was most widely used to monitor morphological changes in the CF lung. However, previous studies demonstrated that, although chest x-ray correlates significantly with PFT parameters, it has a low sensitivity to detect early changes in the CF lung, (Terheggen-Lagro *et al*., 2007) and is inferior to computed tomography (CT). However, compared to chest x-ray, chest CT exposes patients to much higher radiation doses, Brenner & Hall (2007). Considering the necessity of life-long repeated imaging studies, the cumulative radiation dose reached with CT has restricted its use, especially for short-term follow up.

While the trachea and main bronchi are generally well-visualized on MRI, one of the major advantages of MRI is the lack of ionizing radiation which is appealing in evaluating young children and adolescents who may require frequent imaging of the trachea. MRI is also advantageous in imaging tracheal compression or invasion by mediastinal masses or vascular rings or other vascular anomalies that may compress the trachea. Magnetic resonance imaging has therefore been established as a radiation-free alternative to CT and X-rays. Besides morphological imaging, functional qualities of the lung can be visualized and measured regionally. MRI of the chest was proposed as a potential imaging alternative in Cystic Fibrosis patients in the late 1980s, although at that time MRI technology was not capable of producing results comparable to CT.

In the last decade, new technologies and strategies have been implemented to overcome the inherent difficulties of MRI of the lung, Kauczor *et al.* (2001). With the introduction of parallel imaging in clinical practice, faster image acquisition became possible, enabling substantial improvement in temporal and/or spatial resolution. Although spatial resolution is lower as compared to CT, MRI has the advantage of characterizing different aspects of tissue based on different contrasts, as well as enhancement after contrast media administration. Additionally, MRI is capable of visualizing different regional functional aspects of the lung parenchyma (pulmonary hemodynamics, perfusion, ventilation).

In this research work, the mathematical method of using MRI to detect blockage of fluid in cylindrical pipe used by Yusuf *et al.* (2015) is applied to detect the obstruction of flow of oxygen in the lungs resulting in difficulty of breathing. The study adopts magnetic resonance imaging equation to show the mathematical processes involved in detecting tracheomalacia as a disease which occurs in the human trachea with a view to saving human life without surgical operation thereby facilitating medical treatment in a seamless manner.

.

2.0 Mathematical Formulation

Bloch equations have been used to derive the diffusion equation. The second order differential equation so derived, is transformed into cylindrical coordinates to represent the assumed cylindrical structure of the trachea where there is no prevalent disease. This shall serve as Case 1 in the study. Case 2 shall be the diseased portion of the trachea which based on assumption, exhibits reduced radius due to the curved portion of the diseased region. Thereafter, appropriate initial and boundary conditions are applied. The transformed model equation is solved using the method of separation of variables. Radio frequency (RF) field is then introduced into the resultant solution of the equation revealing the response of the diseased portion to the MRI machine.

The x, y and z components Bloch Magnetic Resonance Images equations are:

$$\frac{dM_x}{dt} = -\frac{M_x}{T_2} \tag{1}$$

$$\frac{dM_y}{dt} = \gamma M_z B_1(t) - \frac{M_y}{T_2} \tag{2}$$

$$\frac{dM_z}{dt} = -\gamma M_y B_1(t) - \frac{M_z - M_o}{T_1} \tag{3}$$

where M_0 = equilibrium magnetization

M_x = component of transverse magnetization along the x-axis

M_y = component of transverse magnetization along y-axis

M_z = component of magnetization along the field (z -axis)

γ = gyro-magnetic ratio of fluid spins

$B_1(t)$ = radio-frequency (RF) magnetic field

T_1 = Longitudinal or spin lattice relaxation time

T_2 = Transverse or spin-spin relaxation time (Bloch, 1946)

From the fundamental Bloch equations, Awojoyogbe (2004) evolved the diffusion equation

$$\frac{\partial M_y}{\partial t} = D\frac{\partial^2 M_y}{\partial r^2} + \frac{F_o}{T_p}\gamma B_1(t) \tag{4}$$

where coefficient of diffusion, $D, = -\frac{V^2}{T_p}$,

$T_p = \frac{1}{T_1} + \frac{1}{T_2}$, T_p = Sum of the relaxation rates and

$F_o = \frac{M_o}{T_1}$, F_o =ratio of equilibrium magnetization to spin lattice relaxation time

The diffusion coefficient $D = -\frac{V^2}{T_p}$ was accurately defined in terms of MRI flow parameters fluid velocity,$V, T_1 and\ T_2$ relaxation rates ($T_p = \frac{1}{T_1} + \frac{1}{T_2}$). The absolute value of the fluid velocities for human tissues can be determined with different diffusion coefficient and T_1 , T_2 can be obtained while making appropriate assumptions.

Expressing M_y as

$$M_y = M_y(r, z, t) \tag{5}$$

M_y = transverse magnetization, z = direction of the magnetic field, r = radial axis

It is assumed that a normal trachea has an approximate cylindrical shape. A diseased trachea has a cylindrical shape but the disease portion collapses inward and becomes bean-shaped which in this research work, is being considered as an approximate semi-circle.

In cylindrical polar coordinates,

$$x = rcos\theta,\ y = rsin\theta,\ z = z \tag{6}$$

Hence equation (4) which is a second order non homogenous differential equation becomes

$$\frac{\partial M_y}{\partial t} = D\left(\frac{\partial^2 M_y}{\partial r^2} + \frac{1}{r}\frac{\partial M_y}{\partial r} + \frac{\partial^2 M_y}{\partial z^2}\right) + \frac{F_o}{T_o}\gamma B_1(t) \tag{7}$$

Recall the cylinder is radially symmetric, then it is independent of θ. The general solution to this equation is of the form

$$M_y = F(r, z)U(t) + w_c(t) \tag{8}$$

with $$w_c(\dot{t}) = \frac{F_o}{T_o}\gamma B_1(t) \tag{9}$$

implying $$w_c(t) = \int_0^{t_0} \frac{F_o}{T_o}\gamma B_1(t)\, dt \tag{10}$$

Using the method of separation of variables (MSV),

$$M_y = F(r,z)U(t) \tag{11}$$

The expression on the righthand side of (11) can be written as a product function of $F(r,z)$ and $U(t)$ only. The first function is in terms of (r,z) and the second function is in terms of t only. Both sides must be equal to a constant, say $-\lambda^2$, in order to obtain solution that will not be identically zero. Hence, the following two differential equations evolve:

$$\frac{dU(t)}{dt} + \lambda^2 DU(t) = 0 \tag{13}$$

$$\frac{\partial^2 F}{\partial r^2} + \frac{1}{r}\frac{\partial F}{\partial r} + \frac{\partial^2 F}{\partial z^2} + \lambda^2 F = 0 \tag{14}$$

By integrating equation (13), the general solution is:

$$U(t) = C_1 e^{-\lambda^2 Dt} \quad \lambda = 1, 2, \ldots, \ldots, \tag{15}$$

where C_1 is the arbitrary constant of integration

In order to solve (14), the same method of separation of variables is followed:

$$F = Q(r)Z(z) \tag{16}$$

The expression on the righthand side of (16) can be written as a product function of $Q(r)$ and $Z(z)$ only. The first function is in term of (r) and the second function is in term of z only. Both sides must be equal to a constant, say$-\mu^2$, in order to obtain solutions that will not be identically zero. The following two differential equations evolve;

$$\frac{\partial^2 Q}{\partial r^2} + \frac{1}{r}\frac{\partial Q}{\partial r} + \mu^2 Q = 0 \tag{17}$$

and

$$\frac{\partial^2 Z}{\partial z^2} - \beta^2 Z = 0 \tag{18}$$

where we have

$$\beta^2 = \mu^2 - \lambda^2 \tag{19}$$

From equations (17), a Bessel differential equation evolves and its solution is given as

$$F(r) = C_2 J_0(\mu r) + C_3 Y_m(\mu r) \tag{20}$$

where $J_0(\mu r)$ is the Bessel function of the first kind, of order zero and $Y_m(\mu r)$ is the Bessel function of the second kind, of order m. $C_2 and C_3$ are constants. Also, from (18),

$$Z(z) = C_4 e^{\beta z} + C_5 e^{-\beta z} \tag{21}$$

Consequently, the solutions to the equations are:

$$U(t) = C_1 e^{-\lambda^2 Dt} \quad \lambda = 1, 2, \ldots, \ldots, \tag{22}$$

$$F(r) = C_2 J_0(\mu r) + C_3 Y_m(\mu r) \tag{23}$$

$$Z(z) = C_4 e^{\beta z} + C_5 e^{-\beta z} \tag{24}$$

Combining the solution to the diffusion Equation (7), this gives the product of the quantities in (22), (23) and (24) plus $\int_0^{t_0} w_c(\dot{t})\, dt$

$$\Rightarrow \quad M_y = M_y(r,z,t) = F(r)Z(z)U(t) + \int_0^{t_0} w_c(t)\,dt \qquad (25)$$

$$M_y(r,z,t) = \{C_2 J_0(\mu r) + C_3 Y_m(\mu r)\}\{C_4 e^{\beta z} + C_5 e^{-\beta z}\}\{C_1 e^{-\lambda^2 Dt}\} + \int_0^{t_0} w_c(t)\,dt \quad (26)$$

The initial and boundary conditions are as follows:

$$i)\ M_y(r,z,0) = M_i(r,z);$$

$$ii)\ M_y(r,0,t) = 0;$$

$$iii) M_y(r,L,t) = 0;$$

$$iv) M_y(a,z,t) = 0;$$

$$v)\left|M_y(r,z,t)\right| < M, \qquad (27), \text{Spiegel (1974)}$$

$$M = 1,2,3 \ldots i.e. positive\ integers$$

where r depicts the radius of the normal trachea and a depicts the collapse portion of the diseased trachea and z represents the direction of flow of air (oxygen).

Firstly, $r = 0, Y_m(\mu r) \to -\infty$; to keep the solution finite, C_3 must be zero. Thus,

$$M_y(r,z,t) = \{e^{-\lambda^2 Dt}\}\{C_2 J_0(\mu r)\}\{C_4 e^{\beta z} + C_5 e^{-\beta z}\} \qquad (28)$$

Using the second boundary condition,

$$M_y(r,0,t) = \{e^{-\lambda^2 Dt}\}\{J_0(\mu r)\}\{C_4 + C_5\} = 0 \qquad (29)$$

So that we must have $C_4 + C_5 = 0$ implying that $C_5 = -C_4$ then (28) becomes

$$M_y(r,z,t) = \{e^{-\lambda^2 Dt}\}\{J_0(\mu r)\}\{e^{\beta z} - e^{-\beta z}\} = 0 \qquad (30)$$

From the third condition,

$$M_y(r,L,t) = \{e^{-\lambda^2 Dt}\}\{J_0(\mu r)\}\{e^{\beta L} - e^{-\beta L}\} = 0 \qquad (31)$$

which can be satisfied with $e^{\beta L} - e^{-\beta L} = 0$,

$$\Rightarrow e^{\beta L}.e^{\beta L} = e^{-\beta L}.e^{\beta L} = 1 = e^{2k\pi i} \qquad (32)$$

Note that $$e^{ix} = cosx + isinx \qquad (33)$$

and that implies $e^{2\pi i} = cos2\pi + isin2\pi = 1 = e^{2k\pi i}.\ k = 0,1,2,\ldots\ldots$ (34)

$$\therefore e^{2\beta L} = e^{2k\pi i} \qquad k = 0,1,2,\ldots\ldots \qquad (35)$$

It follows that $2\beta L = 2k\pi i$ or $\beta = \frac{k\pi i}{L},\ k = 0,1,2,\ldots\ldots$ (36)

Using this in (30),

$$M_y(r,L,t) = \{Ce^{-\lambda^2 Dt}\}\{J_0(\mu r)\}sin\frac{k\pi z}{L} = 0 \qquad (37)$$

where C is a new constant.

From the fourth condition, it implies

$$M_y(a,z,t) = \{Ce^{-\lambda^2 Dt}\}\{J_0(\mu a)\}sin\frac{k\pi z}{L} = 0 \quad (38)$$

which can be satisfied only if

$$\{J_0(\mu a)\} = 0 \quad (39)$$

$$\mu a = s_1, s_2, ... \quad (40)$$

$$\mu = \frac{s_1}{a}, \frac{s_2}{a}, ... \quad (41)$$

where $\frac{s_m}{a}(m = 1,2,\ldots.)$.is the positive root of the Bessel function $\{J_0(x)\} = 0$. Now from (19), (36) and (41), it follows that:

$$\lambda^2 = (\frac{s_m}{a})^2 - (\frac{k\pi i}{L})^2 = (\frac{s_m}{a})^2 + (\frac{k\pi}{L})^2 \quad (42)$$

so that a solution satisfying all the boundary conditions except the first is given by

$$M_y(r,z,t) = \left\{Ce^{-Dt(\frac{s_m}{a})^2+(\frac{k\pi}{L})^2}\right\}\left\{J_0\left(\frac{s_m}{a}r\right)\right\}sin\frac{k\pi z}{L} \quad (43)$$

where $k = 1,2,3,\ldots..; m = 1,2,3,....$

Replacing $C\ by\ C_{km}$ and summing over $k\ and\ m$ and by superposition principle

$$M_y(r,z,t) = \sum_{k=1}^{\infty}\sum_{m=1}^{\infty}\left\{C_{km}e^{-Dt(\frac{s_m}{a})^2+(\frac{k\pi}{L})^2}\right\}\left\{J_0\left(\frac{s_m}{a}r\right)\right\}sin\frac{k\pi z}{L} \quad (44)$$

From (28).

$$M_i(r,z) = \sum_{k=1}^{\infty}\sum_{m=1}^{\infty}\{C_{km}\}\left\{J_0\left(\frac{s_m}{a}r\right)\right\}sin\frac{k\pi z}{L} \quad (45)$$

This can be written as

$$M_i(r,z) = \sum_{k=1}^{\infty}[\sum_{m=1}^{\infty}\{C_{km}\}\left\{J_0\left(\frac{s_m}{a}r\right)\right\}]sin\frac{k\pi z}{L} = \sum_{k=1}^{\infty}b_k sin\frac{k\pi z}{L} \quad (46)$$

$$\Rightarrow \quad b_k = \sum_{m=1}^{\infty}\{C_{km}\}\left\{J_0\left(\frac{s_m}{a}r\right)\right\} \quad (47)$$

It follows from this that $b_k$are the Fourier coefficients obtained when $M_i(r,z)$ is expanded into a Fourier sine series in z (r being kept constant).

Thus

$$b_k = \frac{2}{L}\int_0^1 M_i(r,z)sin\frac{k\pi z}{L}dz \quad (48)$$

C_{km} can be found from the expansion in equation (46). Since $b_k$is a function of r this is simply the expansion of b_k into a Bessel series.

Consequently,

$$C_{km} = \frac{2}{J_1^2\left(\frac{S_m}{a}\right)} \int_0^1 r b_k J_0\left(\frac{S_m}{a} r\right) dr \tag{49}$$

Using (47),

$$C_{km} = \frac{4}{J_1^2\left(\frac{S_m}{a}\right) L} \int_0^1 \int_0^1 r M_i(r,z) J_0\left(\frac{S_m}{a} r\right) sin\frac{k\pi z}{L} dr dz \tag{50}$$

The required solution is

$$M_y(r,z,t) = \sum_{k=1}^{\infty} \sum_{m=1}^{\infty} \left\{ C_{km} e^{-Dt\left(\frac{S_m}{a}\right)^2 + \left(\frac{k\pi}{L}\right)^2} \right\} \left\{ J_0\left(\frac{S_m}{a} r\right) \right\} sin\frac{k\pi z}{L} \tag{51}$$

with C_{km}in (49) as coefficient.

With the radio frequency (rf) field, the solution becomes

$$M_y(r,z,t) = \sum_{k=1}^{\infty} \sum_{m=1}^{\infty} \left\{ C_{km} e^{-Dt\left(\frac{S_m}{a}\right)^2 + \left(\frac{k\pi}{L}\right)^2} \right\} \left\{ J_0\left(\frac{S_m}{a} r\right) \right\} sin\frac{k\pi z}{L} + \frac{aF_o}{wT_o} \gamma \sin(wt) \tag{52}$$

Assume $M_i(r,z) = \sigma_0$, a constant.

$$C_{km} = \frac{4\sigma_0}{J_1^2\left(\frac{S_m}{a}\right)} \int_0^1 \int_0^1 r J_0\left(\frac{S_m}{a} r\right) sin\frac{k\pi z}{L} dr dz \tag{53}$$

$$C_{km} = \frac{4\sigma_0}{J_1^2\left(\frac{S_m}{a}\right) L} \left\{ \int_0^1 r J_0\left(\frac{S_m}{a} r\right) dr \int_0^1 sin\frac{k\pi z}{L} dz \right. \tag{54}$$

$$= \frac{4\sigma_0}{J_1^2\left(\frac{S_m}{a}\right)} \left\{ \frac{J_1\left(\frac{S_m}{a}\right)}{\frac{S_m}{a}} \right\} \left\{ \frac{1 - cosk\pi}{k\pi} \right\} \tag{55}$$

$$= \frac{4\sigma_0 (1 - cosk\pi)}{k\pi \frac{S_m}{a} J_1\left(\frac{S_m}{a}\right)} \tag{56}$$

Substituting for C_{km} in equation (51)

$$M_y(r,z,t) = \frac{4\sigma_0}{\pi} \sum_{k=1}^{\infty} \sum_{m=1}^{\infty} \left\{ \frac{(1 - cosk\pi)}{k\pi \frac{S_m}{a} J_1\left(\frac{S_m}{a}\right)} e^{-Dt\left(\frac{S_m}{a}\right)^2 + \left(\frac{k\pi}{L}\right)^2)} \right\} \left\{ J_0\left(\frac{S_m}{a} r\right) \right\} sin\frac{k\pi z}{L} \tag{57}$$

Radio Frequency (RF) transmitter is needed to transmit energy into the sample of the fluid under consideration in order to "activate" the nuclei so that they emit a signal. This is applied as an RF magnetic field $\boldsymbol{B_1(t)}$ where $\boldsymbol{B_1(t)} = bB_1(t)coswt$. This field is said to be linearly polarized, since it oscillates in a single direction. *w* is called the irradiation frequency; it is also the reference frequency of the RF transmitter and the detection system. *w* has value $1x10^8$ rad.s^{-1} (Waldo and Arnold, 1983). Therefore,

$$w_c(t) = \int_0^{t_0} \frac{F_o}{T_p} \gamma B_1(t)\, dt \tag{58}$$

the radio frequency field (rf) is defined as

$$\boldsymbol{B_1(t)} = bB_1(t)coswt \tag{59}$$

$$w_c(t) = \int_0^{t_0} \frac{F_o}{T_p} b\gamma B_1(t)coswt\, dt \tag{60}$$

Hence,

$$\int_0^{t_0} \frac{bF_o}{T_p}\cos(wt)\, dt = \frac{bF_o}{wT_p}\gamma \sin(wt) \tag{61}$$

Consequently, the final solution for the magnetization M_y,of any molecule of oxygen at any point (r, z, t) in the lungs is given as

$$M_y(r,z,t) = \frac{4\sigma_0}{\pi}\sum_{k=1}^{\infty}\sum_{m=1}^{\infty}\left\{\frac{(1-cosk\pi)}{k\pi\frac{s_m}{a}J_1\left(\frac{s_m}{a}\right)}e^{-Dt(\frac{s_m}{a})^2+(\frac{k\pi}{L})^2}\right\}\left\{J_0\left(\frac{s_m}{a}r\right)\right\}sin\frac{k\pi z}{L}$$

$$+\frac{bF_o}{wT_p}\gamma\sin(wt) \tag{62}$$

3.0 Graphical Representation

The graphs of free flow of oxygen along a healthy trachea and along a diseased trachea are presented as follows:

Case 1 – Free Flow of Oxygen	Case 2 – Diseased Condition
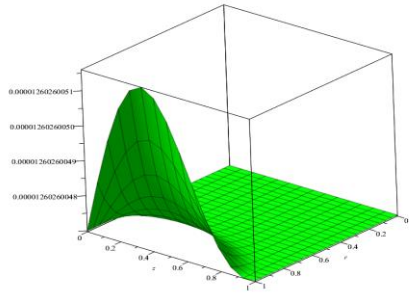 **Figure 1a:** Magnetization against radius and direction of flow when t is $7e^{-14}$	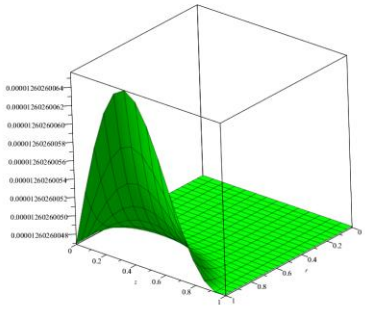 **Figure 1b:** Magnetization against radius and direction of flow when t is $7e^{-14}$
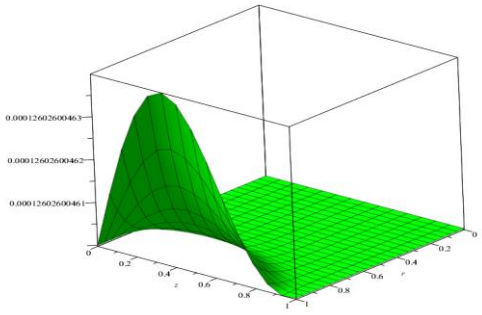	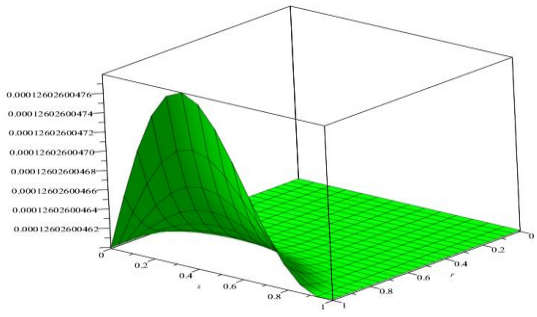

Figure 2a: Magnetization against radius and direction of flow when t is $7e^{-13}$

Figure 2b: Magnetization against radius and direction of flow

when t is $7e^{-13}$

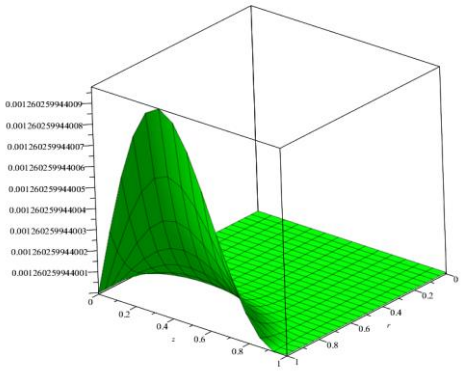

Figure 3a: Magnetization against radius and direction of flow when t is $7e^{-12}$

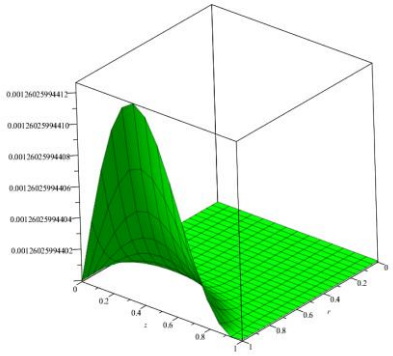

Figure 3b: Magnetization against radius and direction of flow

when t is $7e^{-12}$

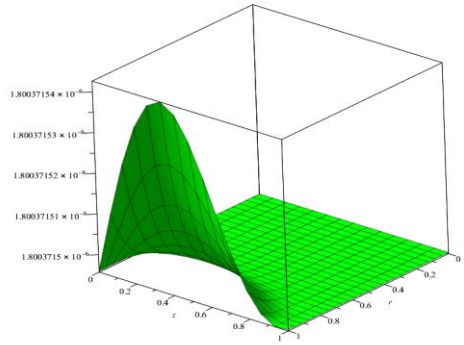

Figure 4a: Magnetization against radius and direction of flow when t is $1e^{-14}$

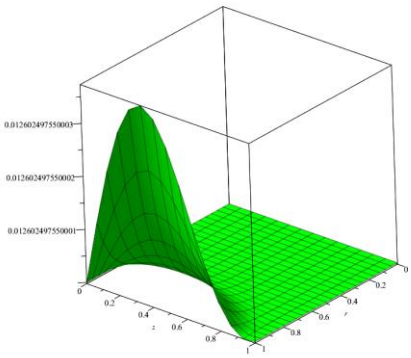

Figure 4b: Magnetization against radius and direction of flow

when t is $7e^{-11}$

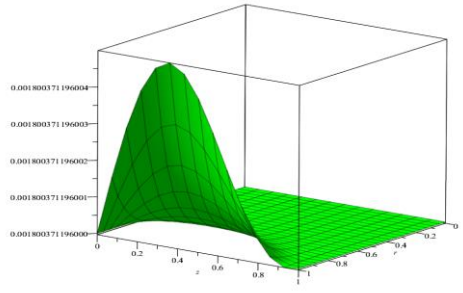

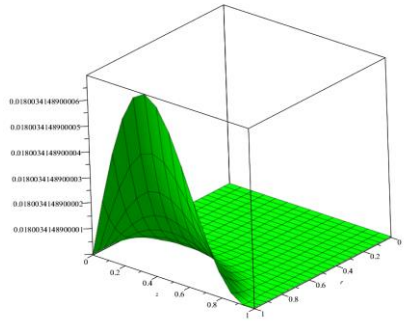

Figure 5a: Magnetization against radius and direction of flow when t is $1e^{-11}$	**Figure 5b:** Magnetization against radius and direction of flow when t is $1e^{-10}$
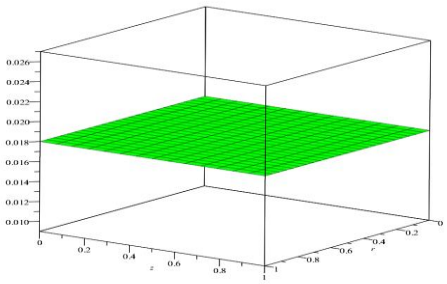 **Figure 6a:** Magnetization against radius and direction of flow when t is $1e^{-10}$	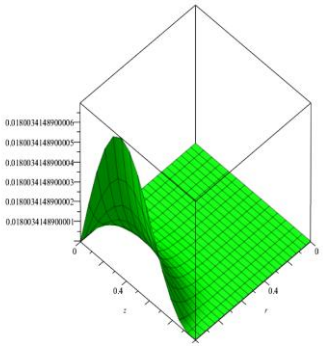 **Figure 6b:** Magnetization against radius and direction of flow when t is $1e^{-9}$

4.0 Discussion

4.1 Discussion on Graphs of Free Flow

Figures 1a to 6a show the graphs of Magnetization plotted against radius (10mm (1cm)) and line of flow in the trachea. The magnetization ranges from 1.26026E-05 to 0.18 (point of relaxation). The graphs demonstrate magnetization values that decayed in accordance with free induction decay (FID) without any sign of obstruction or hinderance both at the inhalation and exhalation stages. This is summarily depicted in Figure 7 and 8. It can be inferred that the manner of decay of the magnetization which is being read as signal lay credence to the fact that there is free flow of oxygen. Hence there is no disease that is prevalent.

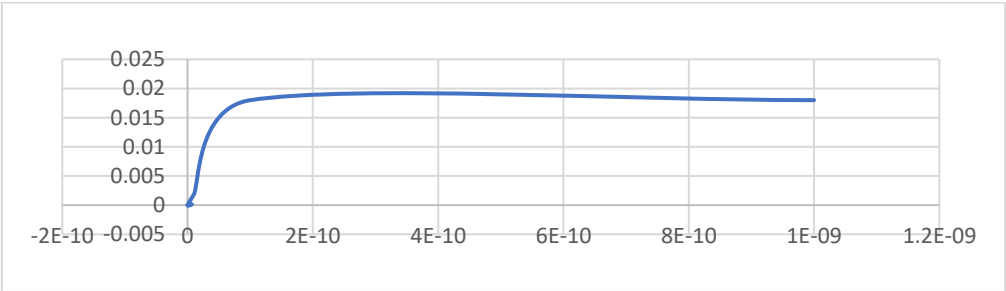

Figure 7: Magnetization against Time for Free flow condition (Normal Trachea during Inhalation)

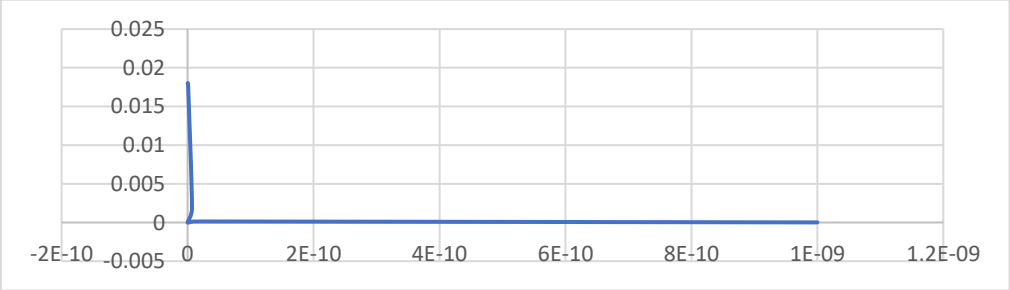

Figure 8: Magnetization against Time for Free flow condition (Normal Trachea during Exhalation)

4.5 Discussion on Graphs of Diseased Condition

Figures 1b to 6b show the graphs of Magnetization plotted against radius ($\frac{r}{a}$ became 5mm (0.5cm)) and line of flow in the trachea. The magnetization ranges from 1.26026E-05 to 1.5 (point of relaxation). The graphs demonstrate an irregularly oblique portion when the magnetization was about to enter relaxation stages of both the inhalation and exhalation stages. This is a sign of obstruction or hinderance at these stages. Figures 9 and 10 summarily depict these two situations. The inference from these is that narrowing of the lung as a result of tracheomalacia is responsible for the unusual shape of the graph.

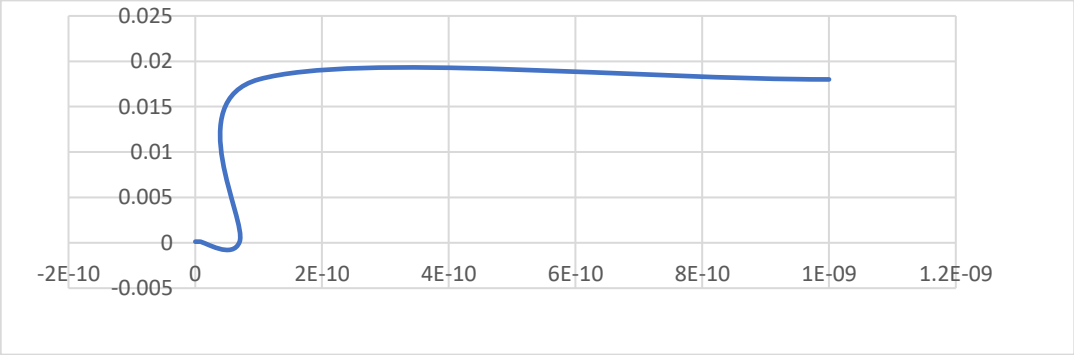

Figure 9: Magnetization against Time for diseased condition (Diseased condition during Inhalation)

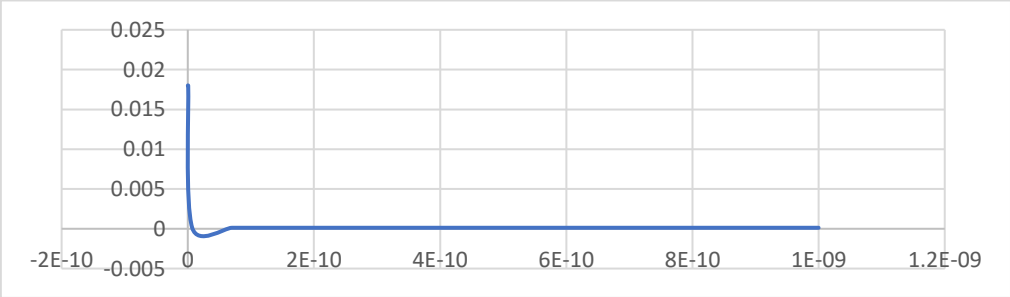

Figure 10: Magnetization against Time for diseased condition (Diseased condition during exhalation)

REFERENCES

Awojoyogbe, O. B., (2004). Analytical solution of the time – dependent Bloch NMR flow equations: A Translational Mechanical Analysis. *Physica A: Statistical Mechanics and its Applications*, 339(3), 437-460, *ISSN 0378-4371*, https://doi.org/10.1016/j.physa.2004.03.061.

Awojoyogbe, O. B. (2009). Analytical solution of the time – dependent Bloch NMR flow equations: A Translational Mechanical Analysis. *Physica A*, 339, 437-460.

Awojoyogbe, O. B, Faromika O. P, Dada, M. & Dada, O. E. (2011). Concepts in magnetic resonance imaging: a review part A. 38(3), 85-101. Published in Wiley online library (wileyonlinelibrary.com). doi:10.1002/cmr.a.20210

Bloch F. (1946). Nuclear induction. Phys Rev 70:460–474.

Brenner D. J. & Hall E. J. (2007). Computed tomography - An increasing source of radiation exposure. *New Engl J Med.*; 357:2277–2284.

Davis S., Jones M. & Kisling J. (2007). Effect of continuous positive airway pressure on forced expiratory flows in infants with tracheomalacia. Am J Respir Crit care med.; 158: 148-152.

Fraga J. C., Jennings R. W. & Kim P. C. W. (2016). Pediatric tracheomalacia. Semin Pediatr Surg.;25(3):156-164.

Kauczor H. U., Chen X. J., van Beek E. J. R. & Schreiber W. G. (2001) *European Respiratory Journal* 17: 1008-1023; DOI**:** 10.1183/09031936.01.17510080.

Klioze, D. (2013). MRI: Basic Physics a Brief History. Retrieved from Youtube: https://www.youtube.com/watch?v=djAxjtN 7VE

Spiegel, M. R. (1974). *Schaum's outline of Fourier analysis with application to boundary value problem*. New York: McGraw-Hill Book Company.

Terheggen-Lagro S. W. J., Arets H. G. M., J. van der Laag & C. K. van der Ent. (2007) *European Respiratory Journal* 30: 279-285; **DOI:** 10.1183/09031936.00051406

Tomassini V. & Palace J. (2009) Multiple sclerosis lesions: insights from imaging techniques. Expert Rev Neurother 9:1341–1359.

Waldo S. H. & Arnold H. L. (1983). An introduction to NMR imaging: From the Bloch equation to the imaging equation. *Proceedings of the IEEE*, 71(3).

Wert, S. E., Polin, R. A.; Abman, S. H.; Rowitch, D. H. & Benitz, W. E. (2017) (eds.), "61 - Normal and Abnormal Structural Development of the Lung"*, Fetal and Neonatal Physiology (Fifth Edition), Elsevier, pp. 627–641.e3,* ISBN 978-0-323-35214-7, retrieved 2021-01-23

Yusuf, S. I., Aiyesimi, Y. M. & Awojoyogbe, O. B. (2010). An analytic investigation of bloch nuclear magnetic resonance flow equation for the analysis of general fluid flow, *Nigerian Journal of Mathematics and Applications*. 20:82-92.

Yusuf, S. I., Aiyesimi, Y. M., Jiya M. & Awojoyogbe, O. B. (2015). Detection of Blockage in a Radially Symmetric Cylindrical Pipe Using Diffusion Magnetic Resonance Equation. *Journal of Science, Technology, Mathematics and Education.* 11(3), 179 – 187.